Inorg. Chem. **2008**, *47*, 3014−3022

Investigation of Primary Crystallite Sizes in Nanocrystalline ZnS Powders: Comparison of Microwave Assisted with Conventional Synthesis Routes

Thomas Rath,[†] Birgit Kunert,[‡] Roland Resel,[‡] Gerhard Fritz-Popovski,[§] Robert Saf,[†] and Gregor Trimmel*[,†]

Institute for Chemistry and Technology of Organic Materials, Graz University of Technology, Stremayrgasse 16, 8010 Graz, Austria, Institute of Solid State Physics, Graz University of Technology, Petersgasse 16, 8010 Graz Austria, and Institute of Chemistry, University of Graz, Heinrichstrasse 28, 8010 Graz, Austria

Received September 10, 2007

ZnS powders with primary crystallite sizes of only a few nanometers were prepared by three different synthesis routes at temperatures below 130 °C. The reaction of zinc acetate dihydrate with thioacetamide (TAA) in the presence of pyridine and triphenylphosphite (TPP) was carried out using either conventional heating or microwave heating. The obtained powders exhibit sphalerite structure as determined by X-ray diffraction (XRD). The primary crystallites have diameters between 1 and 7 nm obtained by XRD. Small angle X-ray scattering (SAXS) measurements were analyzed by the model-free inverse Fourier-transformation approach, as well as by a hard sphere-model from which particle size and polydispersity were extracted. The particle sizes by SAXS are in good agreement with the primary crystallite sizes obtained by XRD. It has been found that an increasing amount of sulfur and/or using microwave heating increases crystallite sizes. The presence of TPP decreases the particle sizes but no significant influence on the TPP concentration was observed. In the alternative third preparation route, hexamethyldisilathiane (HMDST) was used as precipitation reagent at ambient temperature, which leads to the smallest crystallite sizes of only 1 nm together with low polydispersities. Scanning electron microscopy, dynamic light scattering and UV–vis spectroscopy showed that all three synthesis routes lead to ZnS powders with aggregate sizes between 650 and 1200 nm. Both of the TAA-precipitation routes lead to spherical agglomerates which consist of spherical substructures, whereas the HMDST agglomerates are assembled from elongated objects.

Introduction

Nanocrystalline materials have attracted many scientists because of their unique size-dependent thermal, optical, electronic, magnetic, and mechanical properties that differ significantly from their bulk characteristics.[1,2] Among these materials, semiconductors are under the best investigated materials because of the promising possibilities for applications based on their tunable optical and electrooptical characteristics.[3–6]

Zinc sulfide is one of the most important II−VI semiconductors with a band gap of about 3.6 eV.[7] On the one hand, ZnS nanoparticles provide the possibility to study fundamental properties of semiconducting nanoparticles, and, on

* To whom correspondence should be addressed. E-mail: gregor.trimmel@tugraz.at. Phone: ++43316-8734958. Fax: ++43316-8738951.
[†] Institute for Chemistry and Technology of Organic Materials, Graz University of Technology.
[‡] Institute of Solid State Physics, Graz University of Technology.
[§] Institute of Chemistry, University of Graz.

(1) Henglein, A. *Chem. Rev.* **1989**, *89*, 1861.
(2) Trindade, T.; O'Brien, P.; Pickett, N. L. *Chem. Mater.* **2001**, *13*, 3843.
(3) Alivisatos, A. P. *Science* **1996**, *271*, 933.
(4) O'Brien, P., Pickett, N. Strategies for the Scalable Synthesis of Quantum Dots and Related Nanodimensional Materials. In *The Chemistry of Nanomaterials: Synthesis, Properties and Applications*; Rao, C. N. R., Müller, A., Cheetham, A. K., Eds.; Wiley-VCH: Weinheim, 2004; Vol. *1*, pp 12.
(5) Grieve, K.; Mulvaney, P.; Grieser, F. *Curr. Opin. Colloid Interface Sci.* **2000**, *5*, 168.
(6) Rogach, A. L.; Talapin, D. V.; Weller, H. Semiconductor Nanoparticles. In *Colloids and Colloid Assemblies*; Caruso, F., Ed.; Wiley VCH: Weinheim, 2004; pp 52.
(7) Maity, R.; Maiti, U. N.; Mitra, M. K.; Chattopadhyay, K. K. *Physica E* **2006**, *33*, 104.

10.1021/ic7017715 CCC: $40.75
Published on Web 03/20/2008

the other hand, they have a high potential in many different technological applications,[8] for example, as photonic crystals[9,10] or in optoelectronic devices.[11,12]

There are numerous reports on the synthesis of nanocrystalline ZnS in the literature. As examples for low temperature routes, ZnS has been prepared by precipitation methods by mixing zinc salt solutions with sodium sulfide solutions.[11,13–16] Examples of alternative sulfur sources are, for example, thiourea,[17,18] glutathione,[19] hexamethyldisilathiane (HMDST),[20,21] or simple elemental sulfur dissolved in oleylamine.[22,23] A very convenient and often applied synthesis method uses the decomposition of thioacetamide (TAA).[10,24–28] Besides the classical synthesis routes, ultrasonic[29,30] and microwave[31–33] assisted methods have been introduced for the preparation of ZnS-nanomaterials. In general, microwave assisted synthesis routes offer advantages like short reaction times, simplicity of experiments, and energy efficiency.[34–38]

The size of the nanocrystalline semiconductors mainly depends on the preparation conditions. Important parameters are the ratio of metal salt to sulfur source, the presence and amount of a capping ligand, temperature, and aging of the crystals to name only a few. In addition, the crystal structure obtained for nanocrystalline ZnS can be different from the structure usually obtained for the bulk materials. For bulk ZnS, the stable low-temperature phase is the cubic sphalerite (zincblende) structure, whereas for nanocrystalline ZnS it is possible to obtain the high temperature hexagonal wurtzite phase or a mixture of both.[17,19,27,39] The primary ZnS-nanocrystallites often form agglomerates in the micrometer range, for example, as microspheres[10,18,19,24,25,28,40] "self assembled nanoballs"[31] or as hollow structures.[30]

In this contribution we compare a microwave assisted route with two conventional precipitation routes and study the influence of different synthesis parameters on the primary crystallite size. The first route uses TAA as sulfur source and conventional heating,[24] and the second route also uses TAA but microwave heating. To compare the first two methods, we tried to keep the synthesis parameters of these routes as similar as possible. In addition, we investigated an alternative precipitation method at ambient temperature using HMDST $(CH_3)_3Si-S-Si(CH_3)_3$.[41]

The primary crystallite size of the ZnS powders were determined by X-ray diffraction (XRD) and by small-angle X-ray scattering (SAXS). Whereas the XRD measurements give information on the crystalline phase and the primary crystallite size, the SAXS experiments reveal the size of the primary particles and their packing. We thereby focus on the influence of the reaction conditions on the primary crystallite sizes. These crystallites agglomerate and form structures in the micrometer range as revealed by dynamic light scattering (DLS), UV–vis spectroscopy, and scanning electron microscopy (SEM).

Experimental Section

Syntheses. Microwave reactions were carried out in an Anton Paar microwave reaction system Synthos 3000 (800 W, 2.54 GHz). All chemicals were purchased from Sigma Aldrich in the purest form available and used for the syntheses without further purification. All syntheses were carried out under an inert atmosphere. ZnS nanoparticles were prepared according to three general procedures:

Caution! *In the below described reactions, hazardous chemicals and solvents are used (acetonitrile, toluene, pyridine or triphenylphosphite). Precautions have to be taken working with TAA and HMDST as during the synthesis toxic H_2S-gas can be evolved. All reactions must be undertaken under a fume hood and protection clothing must be used.*

Series A: TAA-Precipitation (TAA Route). A mixture of 1.37 mmol $Zn(acetate)_2 \cdot 2H_2O$ (300 mg, 1 equiv), *x* equiv (*y* mL) of

(8) Murugan, A. V.; Heng, O. Y.; Ravi, V.; Viswanath, A. K.; Saaminathan, V. *J. Mater. Sci.* **2006**, *41*, 1459.
(9) Velikov, K. P.; van Blaaderen, A. *Langmuir* **2001**, *17*, 4779.
(10) Liddell, C. M.; Summers, C. J. *J. Colloid Interface Sci.* **2004**, *274*, 103.
(11) Dinsmore, A. D.; Hsu, D. S.; Gray, H. F.; Quadri, S. B.; Tian, Y.; Ratna, B. R. *Appl. Phys. Lett.* **1999**, *75*, 802.
(12) Mach, R.; Müller, G. O. *J. Cryst. Growth* **1990**, *86*, 866.
(13) Vogel, W.; Borse, P. H.; Deshmukh, N.; Kulkarni, S. K. *Langmuir* **2000**, *16*, 2032.
(14) Maity, R.; Chattopadhyay, K. K. *Nanotechnology* **2004**, *15*, 812.
(15) Gilbert, B.; Huang, F.; Lin, Z.; Goodell, C.; Zhang, H. Z.; Banfield, J. F. *Nano Lett.* **2006**, *6*, 605.
(16) Li, H.; Shih, W. Y.; Shih, W.-H. *Nanotechnology,* **2007**, *18*, 205604.
(17) Zhao, Y.; Zhang, Y.; Zhu, H.; Hadjipanayis, G. C.; Xiao, J. Q. *J. Am. Chem. Soc.* **2004**, *126*, 6874.
(18) Wang, W.; Chen, L.; Wang, S.; Xi, B.; Xiong, S.; Qian, Y.; Zhang, Z. *Aust. J. Chem.* **2006**, *59*, 791.
(19) Wu, Q.; Cao, H.; Zhang, S.; Zhang, X.; Rabinovich, D. *Inorg. Chem.* **2006**, *45*, 7316.
(20) Talapin, D. V.; Rogach, A. L.; Kornowski, A.; Haase, M.; Weller, H. *Nano Lett.* **2001**, *1*, 207.
(21) Dabbousi, B. O.; Rodriguez-Viejo, J.; Mikulec, F. V.; Heine, J. R.; Mattoussi, H.; Ober, R.; Jensen, K. F.; Bawendi, M. G. *J. Phys. Chem. B* **1997**, *101*, 9463.
(22) Joo, J.; Na, H. B.; Yu, T.; Yu, J. H.; Kim, Y. W.; Wu, F.; Zhang, J. Z.; Hyeon, T. *J. Am. Chem. Soc.* **2003**, *125*, 11100.
(23) Quan, Z.; Wang, Z.; Yang, P.; Lin, J.; Fang, J. *Inorg. Chem.* **2007**, *46*, 1354.
(24) Scholz, S. M.; Vacassy, R.; Lemaire, L.; Dutta, J.; Hofmann, H. *Appl. Organomet. Chem.* **1998**, *12*, 327.
(25) Scholz, S. M.; Vacassy, R.; Dutta, J.; Hofmann, H.; Akinc, M. *J. Appl. Phys.* **1998**, *83*, 7860.
(26) Wihelmy, D. M.; Matijevic, E. *J.Chem. Soc., Faraday Trans. I* **1984**, *80*, 563.
(27) Zhang, H.; Chen, B.; Gilbert, B.; Banfield, J. F. *J. Mater.Chem.* **2006**, *16*, 249.
(28) Yamaguchi, K.; Yoshida, T.; Lincot, D.; Minoura, H. *J.Phys. Chem. B* **2003**, *107*, 387.
(29) Korotchenkov, O. A.; Cantarero, A.; Shpak, A. P.; Kunitskii, Y. A.; Senkevich, A. I.; Borovoy, M. O.; Nadtochii, A. B. *Nanotechnology* **2005**, *16*, 2033.
(30) He, Y. *Mater. Res. Bull.* **2005**, *40*, 629.
(31) Zhao, Y.; Hong, J.-M.; Zhu, J.-J. *J. Cryst. Growth* **2004**, *270*, 438.
(32) Zhu, J.; Zhou, M.; Xu, J.; Liao, X. *Mater. Lett.* **2001**, *47*, 25.
(33) Yang, H.; Huang, C.; Su, X.; Tang, A. *J. Alloys Compd.* **2005**, *402*, 274.
(34) Mastai, Y.; Gedanken, A., Sonochemistry and Other Novel Methods Developed for the Synthesis of Nanoparticles. In *The Chemistry of Nanomaterials: Synthesis, Properties and Applications*, Rao, C. N. R., Müller, A., Cheetham, A. K., Eds.; Wiley-VCH: Weinheim, 2004; Vol. *1*, p 113.
(35) Grisaru, H.; Palchik, O.; Gedanken, A.; Palchik, V.; Slifkin, M. A.; Weiss, A. M. *Inorg. Chem.* **2003**, *42*, 7148.
(36) Landry, C. C.; Lockwood, J.; Barron, A. R. *Chem. Mater.* **1995**, *7*, 699.
(37) Rao, K. J.; Vaidhyanathan, B.; Ganguli, M.; Ramakrishnan, P. A. *Chem. Mater.* **1999**, *11*, 882.
(38) Qian, H.; Qiu, X.; Li, L.; Ren, J. *J. Phys. Chem. B* **2006**, *110*, 9034.
(39) Zhang, H.; Banfield, J. F. *Nano Lett.* **2004**, *4*, 713.
(40) Huang, F.; Zhang, H.; Banfield, J. F. *Nano Lett.* **2003**, *3*, 373.
(41) Czekelius, C.; Hilgendorff, M.; Spanhel, L.; Bedja, I.; Lerch, M.; Müller, G.; Bloeck, U.; Su, D. S.; Giersig, M. *Adv. Mater.* **1999**, *11*, 643.

triphenylphosphite (TPP, $x = 0, 1, 2, 10, 20$; $y = 0, 0.36, 0.72, 3.6, 7.2$ mL), and 1.1, 2.5, or 5 equiv of TAA (113 mg, 256 mg, or 512 mg) were stirred in 25 mL of toluene and 2 mL of pyridine for 20 min at room temperature to achieve a homogeneous, colorless solution. The mixture was then refluxed for 45 min (oil bath temperature, 180 °C), and during the reaction a colloidal white precipitate was formed. The particles were centrifuged, washed with toluene, acetonitrile, and ethanol, and were dried at 60 °C overnight.

Series B: Microwave Assisted TAA-Precipitation (TAA-MW Route). The microwave reaction vessels were filled with a mixture of 1.37 mmol $Zn(acetate)_2 \cdot 2H_2O$ (300 mg, 1 equiv), x equiv (y mL) of TPP ($x = 0, 1, 2, 10, 20$; $y = 0, 0.36, 0.72, 3.6, 7.2$ mL), 1.1, 2.5, or 5 equiv of TAA (113 mg, 256 mg, or 512 mg), 25 mL of toluene, and 2 mL of pyridine. The vessels were heated with microwave assisted heating to 120 °C for 45 min (starting power 800 W). The particles were centrifuged, washed with toluene, acetonitrile, and ethanol, and were dried at 60 °C overnight.

Series C: HMDST-Precipitation (HMDST Route). A mixture of 1.37 mmol $Zn(acetate)_2 \cdot 2H_2O$ (300 mg, 1 equiv) and x equiv (y mL) TPP ($x = 0, 1, 2, 10, 20$; $y = 0, 0.36, 0.72, 3.6, 7.2$ mL) were stirred in 25 mL of toluene and 2 mL of pyridine for 20 min at room temperature to achieve a homogeneous, colorless solution. A solution of 1.51 mmol (0.32 mL) HMDST in 0.86 mL of toluene was added dropwise at room temperature. The particles were centrifuged, washed with toluene, acetonitrile, and ethanol, and were dried at 60 °C overnight.

Characterization Techniques. XRD patterns were obtained on a Siemens D 501 diffractometer in a Bragg–Brentano geometry operated at 40 kV and 30 mA, using Cu Kα radiation ($\lambda = 1.54178$ Å) at a scan rate of 0.05° (50 s measurement time per step). The average primary crystallite sizes of the ZnS nanoparticles (D_{XRD}) were determined according to the broadening of the diffraction peaks using the Scherrer relationship (eq 1):

$$D_{XRD} \approx \frac{\lambda}{\Delta(2\theta)\cos\theta} \tag{1}$$

where $\Delta(2\theta)$ is the full width at half-maximum (FWHM) of the peak in radians and θ is half of the scattering angle 2θ. In this context it is very important to note that the Scherrer relationship is only a good approximation for spherical crystals. The size is inversely proportional to the FWHM. For the calculation, the 111 reflection at $2\theta = 28.7°$ was used. The experimental line width was determined to be 0.12° at this 2θ position by measuring a Si reference standard (NIST 640c).

The SAXS equipment was a SAXS camera (Anton-Paar, Graz, Austria) using an X-ray generator (Philips, PW 1730/10) operated at 40 kV and 50 mA with a sealed-tube Cu anode. A Göbel mirror was used to convert the divergent polychromatic X-ray beam into a collimated line-shaped beam of Cu Kα radiation. The 2D scattering pattern was recorded by an imaging-plate detector (model Fuji BAS1800 from Raytest, Straubenhardt, Germany) and integrated into the one-dimensional scattering function $I(q)$ using SAXSQuant software (Anton-Paar). The samples were measured at room temperature. The powders were pressed into a 1 mm slit within an Al plate and mounted directly in the camera without using any additional window for the sample holder. The cutoff from the beam stop was at $q = 0.07$ nm^{-1} for the TAA samples and at $q = 0.2$ nm^{-1} for the HMDST samples.

Scanning electron microscopic pictures (SEM) were made on an JEOL JSM-5410 scanning microscope. DLS experiments were carried out using a Malvern Zeta Sizer ZEN 3600 from Malvern Instruments (He−Ne laser with a wavelength of 633 nm and a power of 4.0 mW) in ethanol solutions. UV–vis spectra were measured with a Jasco V-530 UV–vis spectrophotometer.

Theory. SAXS data were evaluated in two ways. The first approach consisted in the Fourier transformation of the scattering intensities $I(q)$ into the pair distance distribution function $p(r)$[42]

$$I(q) = 4\pi \int_0^\infty p(r)\frac{\sin(qr)}{qr}\,dr \tag{2}$$

where q is the absolute value of the scattering vector given by $q = 4\pi/\lambda \sin(\theta)$. Instrumental broadening effects and termination effects of the limited experimental q-scale were minimized by performing an indirect Fourier transformation.[43,44] The $p(r)$ function is interpreted for homogeneous particles as a histogram of distances r within the particle. Aggregates consisting of globular primary particles will therefore show a maximum or shoulder close to the radius of the primary particles.

The second approach of SAXS data evaluation consisted in the approximation of an analytical model to the measured data. The approximation was done by minimizing the mean deviation L defined as

$$L = \frac{1}{M}\sum_{i=1}^{M}\sqrt{\frac{(I_{exp}(q_i) - I_{mod}(q_i))^2}{\sigma^2(q_i)}} \tag{3}$$

where M is the number of data points, $I_{exp}(q_i)$ is the measured scattering intensity of the point at $q = q_i$, $I_{mod}(q_i)$ is the corresponding intensity of the model, and σ the standard deviation of the measured point. The parameter combination corresponding to the global minimum in L and therefore defining the best approximation was searched by a Boltzmann-Simplex Simulated Annealing algorithm.[45] The limits of uncertainty of the fit parameters were estimated by creating 10 artificial data sets, where random errors were added to the measured data according to the experimental standard deviations of the experimental points. These data sets were evaluated with the same model, and the standard deviation of the corresponding resulting parameters from the ones obtained from the original data set was calculated.[46]

The model was based on the one introduced by Hoekstra and co-workers for sticky hard spheres in shear flow,[47] which was used for powders for the first time by Jensen et al.[48] The model assumes that the form factor describing the scattering of the individual particles $P(q)$ and the structure factor $S(q)$, which describes the influence by particle arrangement, can be separated as follows[49]

$$I(q) = nP(q)\,S(q) \tag{4}$$

While the form factor is the one of a sphere,[50] the structure factor is given by the sum

$$S(q) = S_p(q) + S_f(q) \tag{5}$$

where $S_p(q)$ is the part describing direct particle interactions, which can be done by means of the analytical Percus-Yevick approxima-

(42) Porod, G. *Acta Phys. Austriaca* **1948**, *2*, 255.
(43) Glatter, O. *Acta Phys. Austriaca* **1977**, *47*, 83.
(44) Glatter, O. *J. Appl. Crystallogr.* **1977**, *10*, 415.
(45) Press, W. H.; Teukolsky, S. A.; Vetterling, W. T.; Flannery, B. P. *Numerical Recipes in Fortran 77*; Cambridge University Press: Cambridge, 1997; Vol *1*.
(46) Svergun, D. I.; Pedersen, J. S. *J. Appl. Crystallogr.* **1994**, *27*, 241.
(47) Hoekstra, H.; Mewis, J.; Narayanan, T.; Vermant, J. *Langmuir* **2005**, *21*, 11017.
(48) Jensen, H.; Pedersen, J. H.; Jørgensen, J. E.; Pedersen, J. S.; Joensen, K. D.; Iversen, S. B.; Søgaard, E. G. *J. Exp. Nanosci.* **2006**, *1*, 355.
(49) Zernike, F.; Prins, J. A. *Z. Phys.* **1927**, *41*, 184.
(50) Lord Rayleigh, J. W. *Proc. R. Soc. London* **1911**, *A84*, 25.

tion for hard spheres.[51] The fractal structure of the whole aggregate is then described by $S_f(q)$, which was computed using the equation given by Teixeira.[52]

The original model was slightly modified by introducing polydispersity as the FWHM of a Schultz distribution of the particle size.[53] The polydispersity was handled according to the local monodisperse approximation[54]

$$I_{mod}(q) = \int_0^\infty P(q,r)\, S(q,r)\, N(r)\, dr \qquad (6)$$

where $N(r)$ is the size distribution giving the weight of the particle contribution of radius r. Finally, instrumental broadening effects were introduced by convoluting the calculated scattering curve of the model with the beam width and the beam length profiles of the primary beam.[55]

Results and Discussion

In this work three different synthesis routes for ZnS powders were investigated with experimental parameters as similar as possible. For the first two approaches, zinc acetate dihydrate and TAA were dissolved in pyridine. Then the appropriate amount of TPP and toluene was subsequently added to this solution. In the first route, the TAA-precipitation route (TAA), the solution was heated up till a constant reflux of the solvent was reached (approximately 15 min). While the mixture was refluxed for 45 min, the ZnS powder precipitates as a white solid. In the second route, the TAA-microwave assisted route (TAA-MW), the solution was irradiated in a microwave reaction system with a starting power of 800 W, which is then continuously reduced to keep the temperature constant. The temperatures in the reaction flasks were measured with an IR-thermo sensor to be at around 120 °C, near the refluxing temperature of toluene. In both synthesis routes, the sulfide is generated by thermal decomposition of TAA. Under basic conditions—the reaction mixture contains pyridine and a small quantity of water stemming from the dihydrate of zinc acetate—and in the presence of Zn^{2+}, a direct reaction between the metal and the TAA is assumed that leads to the formation of ZnS and the release of acetonitrile.[27]

The third synthesis route uses HMDST as sulfur source. This has the advantage that the reaction can be carried out at ambient temperature as HMDST readily decomposes. In this route, zinc acetate dihydrate was dissolved in pyridine, toluene, and the appropriate amount of TPP. After 15 min stirring, HMDST was added dropwise to the colorless solution within 10 min. After the addition of 20% of HMDST, a white powder started to precipitate.

For a detailed comparison of the three methods, the amount of added TPP was varied from 0 to 20 equiv and the amount of added TAA was varied from 1.1 to 5 equiv. In the case of HMDST, only the amount of TPP was varied as the use of a big excess of HMDST was not practicable because of the offensive smell generated by this reaction. In addition, the amount of HMDST was added dropwise, whereas in both the other routes, TAA was added at once at the beginning. The samples were labeled as follows: SR-x_{Sulfur}/y_{TPP} with SR as the synthesis route, TAA for the thermal TAA route, TAA-MW for the microwave assisted TAA route, and HMDST for the HMDST route—x_{Sulfur} as the amount of sulfur equivalent in reference to Zn and y_{TPP} as the equivalent amount of TPP; for example, TAA-MW-2.5/2 is the sample prepared according to the microwave assisted route with 2.5 equiv of TAA and 2 equiv of TPP.

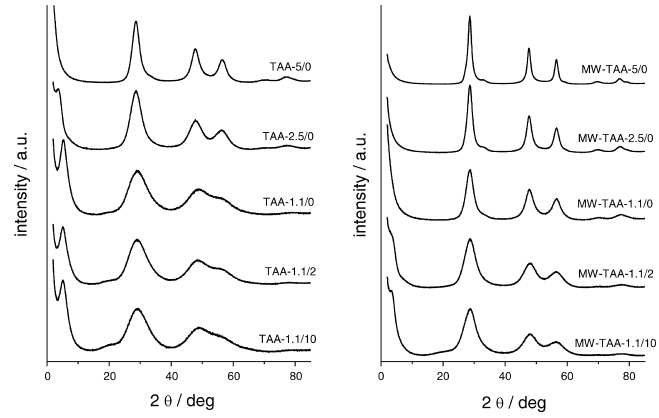

Figure 1. XRD patterns of the ZnS-samples prepared via the TAA route (left side) and the TAA-MW route (right side). The curves are vertically shifted for better visibility.

In all three cases, white ZnS powder precipitates during the synthesis. In the case of TAA and TAA-MW, the precipitates are more compact, whereas the HMDTS route yields a more flocculent product. The powders were centrifuged from the reaction mixture and subsequently washed with toluene, acetonitrile, and ethanol to remove residual organic compounds and salts.

For the analysis of the primary crystallite size, the as-prepared ZnS nanoparticles were characterized by XRD and SAXS measurements.

Figure 1 compares representative XRD patterns of ZnS nanoparticles prepared by the TAA-precipitation with the corresponding patterns of microwave assisted TAA-precipitation samples. The sharpest peaks are observed in the pattern of sample TAA-MW-5/0 in which the highest amount of TAA and no TPP were used. Intense peaks at 28.7° (111), 47.6° (220), 56.3° (311), and smaller ones at 33.1° (200), 59.1° (222), 69.5° (400), 76.8° (331), and 79.1° (420) are observed, which are in good agreement to the Powder Diffraction File (PDF) 5–0566 of the International Centre for Diffraction Data for sphalerite-ZnS. Using the Scherrer equation, eq 1, one can estimate a primary crystallite size of about 7.1 nm. Using lower amounts of TAA and/or using TPP during the microwave assisted synthesis, one observes that the peaks become broader indicating smaller primary crystallite sizes. The powders obtained by conventional heating always exhibit lower crystallite sizes than those prepared by TAA-MW. For example, the crystallite size of the sample with the same chemical composition TAA-5/0 is estimated to be only 3.4 nm—that is half of the size of TAA-MW-5/0. The sample with the lowest crystallite size is TAA-1.1/20 which exhibits a value of 1.0 nm. In this case the

(51) Percus, J. K.; Yevick, G. J. *Phys. Rev.* **1958**, *110*, 1.
(52) Teixeira, J. *J. Appl. Crystallogr.* **1988**, *21*, 781.
(53) Schulz, G. V. *Z. Phys. Chem. Abt. B* **1939**, *43*, 25.
(54) Pedersen, J. S. *J. Appl. Crystallogr.* **1994**, *27*, 595.
(55) Kratky, O.; Porod, G.; Skala, Z. A. *Acta Phys. Austriaca* **1960**, *13*, 76.

Table 1. Characteristic Data of the ZnS-Samples Prepared via the TAA route Obtained by XRD[a] and by SAXS Measurements[b]

			XRD		SAXS			
					$p(r)$	model		
TAA	TPP	sample	D_{XRD}, nm	a, Å	D_{IFT}, nm	D_{HSM}, nm	app. vol. frac.	app. polydisp.
1.1	0	TAA-1.1/0	1.4	5.29	1.1	1.5	0.45	0.22
	1	TAA-1.1/1	1.3	5.35	1.1	1.4	0.44	0.23
	2	TAA-1.1/2	1.3	5.30	1.0	1.5	0.50	0.25
	10	TAA-1.1/10	1.3	5.29	1.0	1.5	0.45	0.20
	20	TAA-1.1/20	1.0	5.14	1.1	1.3	0.40	0.15
2.5	0	TAA-2.5/0	2.0	5.38	2.0	1.3	0.18	0.46
	2	TAA-2.5/2	1.8	5.36	1.4	1.1	0.23	0.46
	10	TAA-2.5/10	1.5	5.37	1.2	1.3	0.25	0.26
5	0	TAA-5/0	3.4	5.38	4.8	4.5	0.63	0.76
	2	TAA-5/2	2.5	5.38	3.4	1.5	0.28	0.40
	10	TAA-5/10	1.7	5.38	1.4	1.3	0.10	0.12

[a] D_{XRD}, diameter of the primary crystallites estimated by eq 1 using the 111 reflection at $2\theta = 28.7°$; a, lattice constant. [b] D_{IFT}, primary particle size calculated from the $p(r)$-function; primary particle size D_{HSM}, apparent volume fraction, and apparent polydispersity calculated by the hard sphere model.

Table 2. Characteristic Data of the ZnS-samples Prepared via the TAA-MW Route Obtained by XRD[a] and by SAXS Measurements[b]

			XRD		SAXS			
					$p(r)$	model		
TAA	TPP	sample	D_{XRD}, nm	a, Å	D_{IFT}, nm	D_{HSM}, nm	app. vol. frac.	app. polydisp.
1.1	0	TAA-MW-1.1/0	3.1	5.38	5.8	2.2	0.59	0.37
	1	TAA-MW-1.1/1	2.0	5.36	1.4	1.6	0.32	0.37
	2	TAA-MW-1.1/2	2.0	5.37	2.0	1.4	0.10	0.33
	10	TAA-MW-1.1/10	1.8	5.37	1.8	1.5	0.34	0.35
	20	TAA-MW-1.1/20	2.0	5.40	2.0	2.2	0.42	0.28
2.5	0	TAA-MW-2.5/0	4.8	5.39	6.0	1.7	0.15	1.46
	2	TAA-MW-2.5/2	2.0	5.38	1.6	1.6	0.13	0.27
	10	TAA-MW-2.5/10	2.2	5.38	2.6	2.0	0.29	0.32
5	0	TAA-MW-5/0	7.1	5.40	9.8	4.3	0.64	0.61
	2	TAA-MW-5/2	2.4	5.38	3.0	1.4	0.38	0.66
	10	TAA-MW-5/10	2.4	5.36	3.4	1.7	0.25	0.70

[a] D_{XRD}, diameter of the primary crystallites estimated by eq 1 using the 111 reflection at $2\theta = 28.7°$; a, lattice constant. [b] D_{IFT}, primary particle size calculated from the $p(r)$-function; primary particle size D_{HSM}, apparent volume fraction, and apparent polydispersity calculated by the hard sphere model.

220 and 311 peaks are merging together, and the low intensity peaks are hardly seen. The X-ray patterns of this sample, as well as of sample TAA-1.1/10, seem to be rather similar to the X-ray pattern of nanocrystalline hexagonal ZnS (wurtzite). However, in comparison with literature data,[17] the (100) and (101) planes as well as the (110) and (112) planes are not pronounced strongly enough to interpret the structure of TAA-1.1/10 as a wurtzite structure (cf. PDF 79–2204). Therefore, we assume that this sample does not consist of hexagonal ZnS but more likely of cubic ZnS (sphalerite) with a small size of the crystallites. Considering a primary crystallite size of about 1.0 for the smallest crystallites and keeping in mind that the length of the unit cell of cubic ZnS is about 0.54 nm, there is only short periodicity in the material.

The primary crystallite size (D_{XRD}) obtained by eq 1 for both of the series are summarized in Table 1 for the TAA route and in Table 2 for the TAA-MW route.

The powders prepared by the HMDST route show similar X-ray patterns as the sample TAA-1.1/10 and exhibit the smallest primary crystallite sizes (see Figure 2). The estimation of the crystallite size gives values below 1.3 nm for all samples as summarized in Table 3.

The XRD pattern of the HMDST samples cannot be attributed unambiguously to cubic sphalerite as the reflections are general broad and not resolved. The identification of the "real" structure of such extremely small crystals is extremely laborious, and the differentiation between the cubic and the hexagonal phase, a mixture of both, a defect phase, and a "liquid-like structure with the short range order of bulk ZnS" as proposed by Vogel et al.[13] for ZnS nanoparticles of similar size, remains often unsolved. A nanoparticle of 1 nm size only contains approximately 30 ZnS units, and more than half of the atoms are located at the surface. To our point of view, the cubic phase is still present in these samples, but the whole lattice structure is distorted by the large surface. A further hint of the presence of an initial sphalerite structure

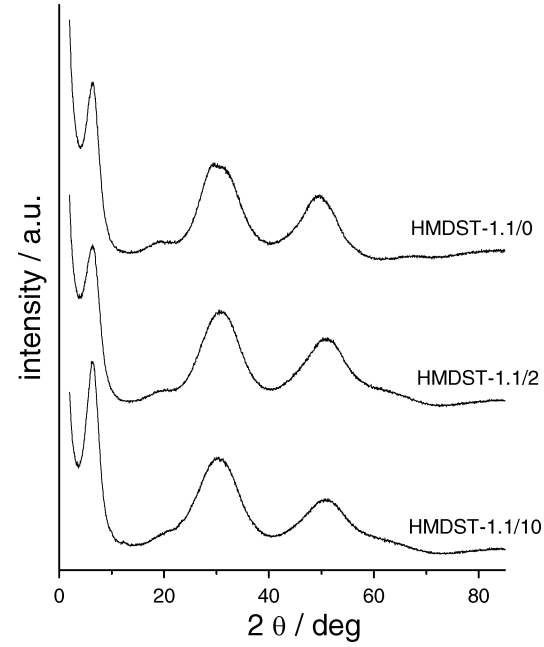

Figure 2. Diffraction patterns of the ZnS nanoparticles prepared by the HMDST route. The curves are vertically shifted for better visibility.

is obtained by an annealing experiment. Sample HMDST-1.1/2 was heated to 300 °C under an inert atmosphere. The XRD pattern of this sample, attached to the Supporting Information, shows the characteristic features for cubic structure with a crystallite size of approximately 4 nm.

All the samples, especially those with small primary crystallite sizes, show a slight deviation of the 2θ values in comparison with the reference diffraction pattern PDF 5–0566. A shift to higher 2θ values is observed. Using the measured d values of the 111 reflection, the lattice constants of the samples were calculated and included in Tables 1−3. The lattice constant a is smaller than that of the bulk ZnS for all samples. At the first glance, it is obvious that smaller crystallites give smaller lattice constants. This is graphically depicted in Figure 3, in which the lattice constant a is plotted versus the crystallite size.

Table 3. Characteristic Data of the ZnS Samples Prepared via the HMDST Route Obtained by XRD[a] and by SAXS Measurements[b]

			XRD		SAXS			
					$p(r)$	model		
HMDST	TPP	sample	D_{XRD}, nm	a, Å	D_{IFT}, nm	D_{HSM}, nm	app. vol. frac.	app. polydisp.
1.1	0	HMDST-1.1/0	1.2	5.09	1.2	1.3	0.41	0.14
	1	HMDST-1.1/1	1.1	5.09	1.3	1.2	0.36	0.12
	2	HMDST-1.1/2	1.3	5.03	1.2	1.2	0.38	0.15
	10	HMDST-1.1/10	1.1	5.10	1.2	1.3	0.42	0.15
	20	HMDST-1.1/20	1.1	5.12	1.2	1.3	0.34	0.00

[a] D_{XRD}, diameter of the primary crystallites estimated by eq 1 using the 111 reflection at $2\theta = 28.7°$; a, lattice constant. [b] D_{IFT}, primary particle size calculated from the $p(r)$-function; primary particle size D_{HSM}, apparent volume fraction, and apparent polydispersity calculated by the hard sphere model.

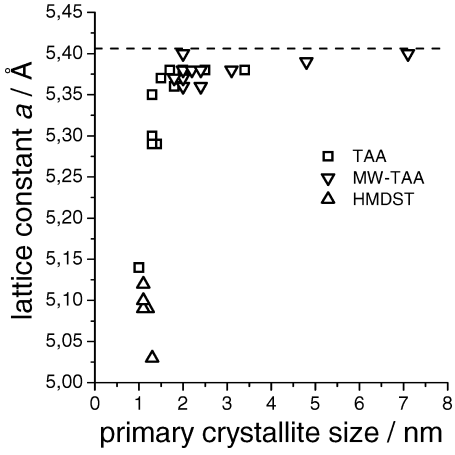

Figure 3. Primary crystallite size vs lattice constant (dashed line represents the lattice constant of bulk ZnS, $a = 5.406$ Å).

The dashed line represents the lattice constant of bulk ZnS, $a = 5.406$ Å, according to PDF 5–0566.

There are several possible explanations for such a peak shift. The first one is that it is caused by an experimental effect related to the 2θ dependence of the atomic scattering function. However, this can be excluded as the peak maximum would then be shifted to lower 2θ angles.[56]

A peak shift to lower or higher scattering angles could be affected by the small impurities of the used reagents. However, this seems not very likely because the same chemicals were always used in all reactions. Another possibility to explain this peak shift is the polymorphism of the zinc sulfide. If there are small amounts of wurtzite structure in the sphalerite-ZnS the peaks could be shifted. However, there are no peaks observed which can be definitely attributed to the wurtzite structure.

Therefore, the mechanism most likely to explain the peak shift is related with cluster surface relaxation. This effect plays an increased role when the primary crystallite size decreases and the surface/volume ratio becomes higher. The surface relaxation leads to contraction of the lattice in nanocrystals. This effect was investigated theoretically and experimentally for nanocrystalline Pd particles.[57] Because of the extreme small crystallite size of the here investigated samples, this explanation seems to be the most appropriate.

In almost every diffraction pattern of the prepared samples, a weak broad peak around $2\theta = 20°$ is observed. This peak derives from the short-range order of organic material like pyridine or TPP incorporated in the ZnS powder.

In samples exhibiting a primary crystallite size less than 2 nm, an additional peak is observed in the low 2θ range of the diffractogram, for example, TAA-1.1/10 (Figure 1) and especially all HMDST samples (Figure 2). This peak does not derive from the sphalerite structure of the material but indicates an overall structural feature of the samples. This peak is remarkably sharp for many samples. The exact peak position correlates quite well with the crystallite size calculated by eq 1. We interpret this peak to be a result of the particle dimension in the low scattering regime. In the range $2\theta < 5°$, the experimental uncertainties of the measurements that have been carried out are too high for the exact analysis of the particle size. Therefore, SAXS measurements were undertaken. In Figure 4, representative small angle scattering curves for all three series are shown. All curves show a pronounced upturn at low q, which can be attributed to the scattering of large aggregates formed by small primary particles. Most of the curves show also a peak or shoulder at larger scattering angles, which is caused by the size and shape of the primary particles and their local arrangement relative to each other. This peak correlates well with the reflection at $2\theta < 5°$ in the corresponding XRD patterns.

As a first evaluation approach, the SAXS curves were analyzed by an indirect Fourier transformation (IFT) which has the advantage that it is a model free approach. In the case of homogeneous, monodisperse spheres, the obtained $p(r)$ function shows a maximum at a distance r close to the radius of the spheres. This behavior is also preserved for aggregates made from spherical subunits, where such a maximum can still be observed at about the distance that corresponds to the radius of the primary particles. The exact arrangement of the particles with respect to each other and, especially, their polydispersity can cause a broadening of the peak, which will lead to a shoulder instead of a peak.

The inner part of the $p(r)$ functions obtained by the IFT analysis for the TAA-MW series represented in Figure 4b is shown in Figure 5. In many cases, one can observe the expected peak, although TAA-MW-1.1/2 and TAA-MW-1.1/10 show only shoulders, which makes a precise estimation of the radii difficult. This behavior can be seen as an indication for the rather polydisperse sizes of the primary crystallites.

The diameters of the nanoparticles obtained from the first maximum of the $p(r)$-function D_{IFT} are included in Tables 1−3.

The second evaluation approach of the SAXS data is based on the hard sphere model. While this method has the advantage of resulting in numbers for radii, as well as for other parameters like polydispersity and apparent volume fraction, it is limited in its scope by the flexibility of the model. The samples could be evaluated, and the diameter

(56) Kaszkur, Z. *Z. Kristallogr.* **2006**, 147.
(57) Kaszkur, Z. *J. Appl. Crystallogr.* **2000**, *33*, 1262.

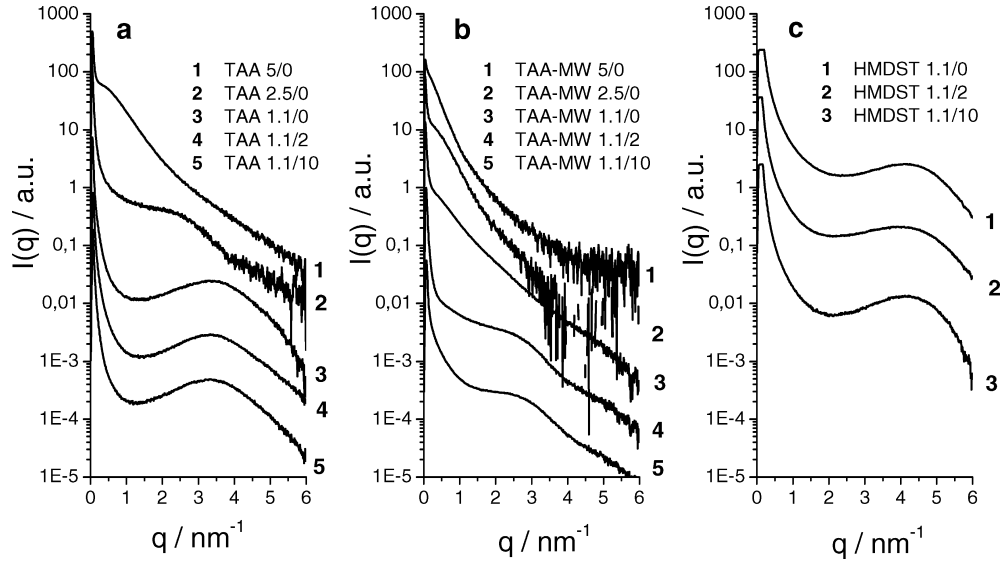

Figure 4. SAXS data of representative samples of the three synthesis routes (a) TAA, (b) TAA-MW, and (c) HMDST. The curves are vertically shifted for better visibility.

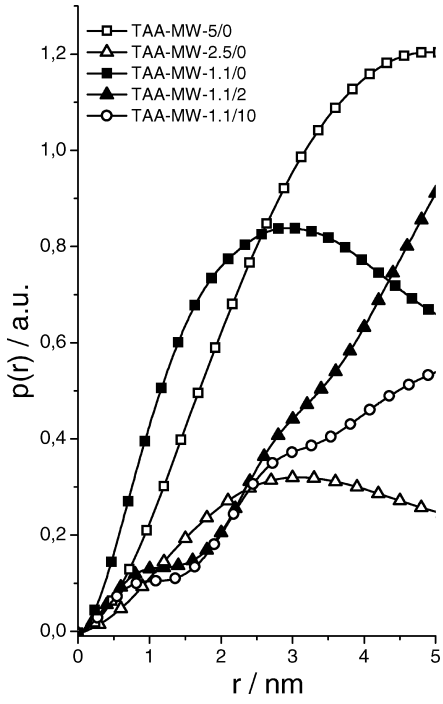

Figure 5. SAXS data of the TAA-MW series after IFT.

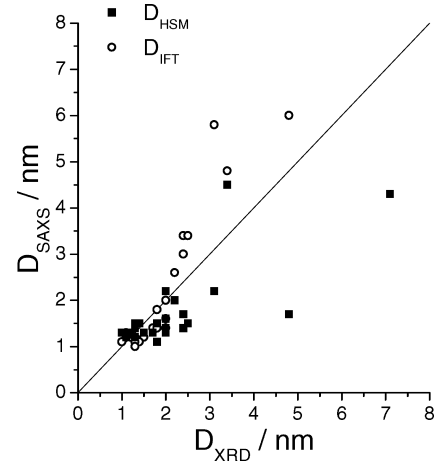

Figure 6. Comparison of primary crystallite sizes estimated by the Scherrer formula (D_{XRD}) and primary particle sizes calculated from SAXS data D_{SAXS} (model, D_{HSM}, and indirect Fourier transformation, D_{IFT}). The straight line gives the perfect correlation.

of the particles, D_{HSM}, the apparent polydispersity as a value for the dispersity of the particle sizes, and the apparent volume fractions are included in Tables 1−3. Fit ranges for the SAXS model, mean deviation, and limits of uncertainty of the fit parameters are given in the Supporting Information. We have to stress that changes in volume fraction hardly change the scattering behavior for volume fractions above 0.3. Polydispersity can also influence this value because it mainly depends in this model on $S_p(0)$.[58] Therefore, it is most likely not the real volume fraction of the nanoparticles within the aggregates but some kind of "apparent volume fraction", which can only be used as a rough estimate. The polydispersity itself is also only an apparent value, because the model takes only a polydispersity in size into account. According to Mittelbach and Porod, it is however impossible to distinguish between polydispersity in size and deviation from perfect spherical geometry of the particles.[59]

A comparison of the data in Tables 1−3 shows that in most cases the particle size obtained by SAXS agrees with the crystallite size determined by XRD, which is graphically depicted in Figure 6. This means that the primary crystallites, seen by XRD, are identical with the primary particles observed by SAXS.

The calculations from both XRD and SAXS measurements are influenced by several factors. In case of the XRD calculations, defects, uncertainties of the exact phase, irregular shape, and polydispersity of the crystallites can cause deviations. Using the low angle regime in SAXS, the particle size can be determined irrespectively from the crystal phase; however, difficulties due to shape and polydispersity are even

(58) Weyerich, B.; Brunner-Popela, J.; Glatter, O. *J. Appl. Crystallogr.* **1999**, *32*, 197.

(59) Mittelbach, P.; Porod, G. *Acta Phys. Austriaca* **1962**, *15*, 122.

more pronounced. Nevertheless, general trends of size changes due to experimental conditions can be observed from these data.

All investigated preparation conditions lead to the formation of nanocrystalline ZnS powders. It is interesting, that samples without TPP also lead to nanocrystalline ZnS. However, in the TAA-MW series a significant difference between the samples with and without TPP is observed. Using the same amount of TAA, the samples with TPP show lower crystallite sizes. The same can be observed for the TAA route with 2.5 and 5 equiv of TAA, whereas there are no differences observed in the case of the TAA-1.1/*y* and the HMDST samples. Unexpectedly, the amount of capper does not have a significant influence on the primary particles by the constant amount of the sulfur component. Using the D_{XRD} values, the crystallite size increases with increasing TAA concentration. Microwave irradiation leads to even larger crystallites. The HMDST preparation route gives in all cases the smallest *d*-values. In addition, the polydispersity of all HMDST samples is very low, indicating the uniformity of the primary particle sizes. The apparent volume fraction shows that the hard sphere packing is not as dense as expected, probably because of the organic capping reagents that are present in the samples. The theoretical limit for randomly densely packed hard spheres should be 0.63 for monodisperse hard spheres, but usually this value is not reached because at a volume fraction of 0.58 a glass is formed.[60,61] Polydisperse spheres, however, can reach more densely packed arrangements. The main differences of the HMDST route to the TAA and TAA-MW routes are the lower temperature during synthesis and the controlled and slow addition of the sulfur source. Therefore, sulfur is always the limiting factor of the crystal growth. This factor seems to be dominant, and no influence on the TPP concentration is observed.

Looking at the TAA and TAA-MW samples, the crystallite size increases with the amount of TAA, supporting the idea that the availability of sulfur is the main factor. Comparing the corresponding TAA with the TAA-MW samples, the microwave assisted route leads to bigger crystallites. As microwave reactions are known to proceed faster, it seems conclusive that the decomposition of TAA takes place more rapidly by increasing the starting sulfur concentration, which leads to a faster crystal growth. In addition, the values of the apparent polydispersities for the TAA and, especially, for the TAA-MW samples are generally higher than for the HMDST route, meaning that the crystallites are not uniform in size.

Investigation of the Aggregate Size of the ZnS Powders. Although the primary crystallite size is always in the nanometer range, aggregates are formed in the investigated samples. DLS was used to evaluate the size of these powders. For this purpose, ZnS suspensions in different solvents (ethanol, toluene, acetonitrile) were prepared. However, because of the instability of the suspension, the measurements were very difficult to reproduce. The ZnS aggregates tend to further agglomerate and to precipitate from the solvent. The main conclusion from the performed experiments is that in all cases the size of the agglomerates exhibit diameters between 650 and 1200 nm. Representative DLS data are presented in the Supporting Information.

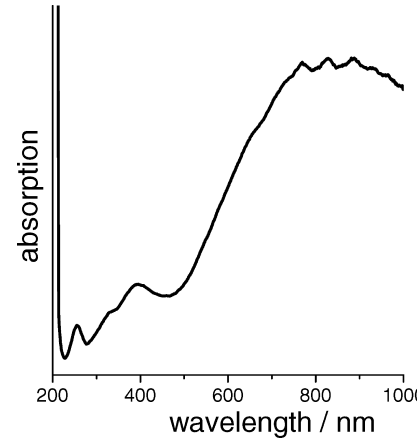

Figure 7. UV–vis spectrum of TAA-MW-2.5/0.

The formation of agglomerates is also observed in the UV–vis spectra. A typical spectrum is depicted in Figure 7. The small maximum at 255 nm stems from the residual pyridine or TPP enclosed in the agglomerates or coordinated to the crystallite core. The presence of these organic compounds is also proven by FTIR measurements (a representative spectrum is given in the Supporting Information). The UV–vis-spectrum is dominated by several broad peaks between 300 and 1000 nm, showing additionally some fine oscillations, which are typically for effects caused by Mie scattering on spherical particles. According to Mie theory, dielectric spheres with a radius comparable to the wavelength of the light are efficient scatterers, and several authors have used this theory to calculate the agglomerate size.[10,18,24,25] Comparing our data with similar spectra, values from 500 to 1000 nm can be estimated; however, because of the instability of the solutions, the quality of the recorded spectra on one hand and the polydispersity of the agglomerate size on the other hand does not allow exact calculations using the Mie theory.

To get a deeper insight, we undertook SEM investigations of representative samples. Figure 8 shows exemplary SEM images. The primary particles form agglomerates of about 1000 nm which correlate well to the DLS and UV–vis measurements. Samples prepared according to the TAA-MW route (Figure 8A,B) show well defined, spherical agglomerates which form a compact mass. Figure 8C, a magnification of Figure 8B, shows the assembly of spheres with a pronounced polydispersity in size with additional small features on the surface in the range of 50 to 150 nm. Similar spherical aggregates have been observed by several other groups.[10,18,19,25,28,40]

The samples prepared according to the TAA route (Figure 8D,E) consist mainly of spherical particles but with additional angled objects and are not as closely packed as the TAA-MW-agglomerates. In both routes, samples prepared with

(60) Van Mengen, W.; Underwood, S. M. *Phys. Rev. E* **1994**, *49*, 4206.
(61) Phan, S.-E.; Russel, W. B.; Cheng, Z. D.; Zhu, J. X.; Chaikon, P. M.; Dunsmuir, J. H.; Ottewill, R. H. *Phys. Rev. E* **1996**, *54*, 6633.

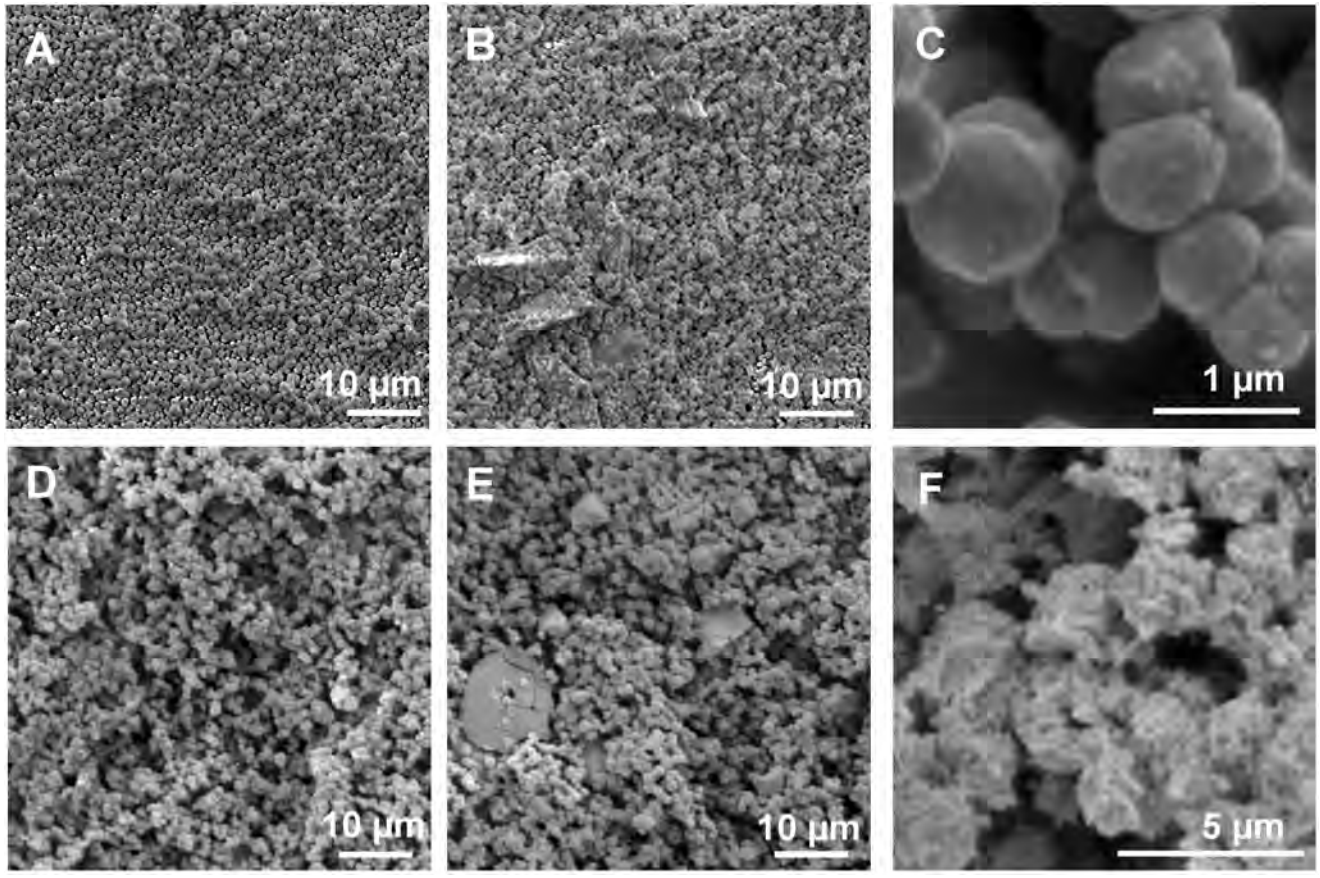

Figure 8. SEM images of the prepared ZnS powders: (A) TAA-MW-1.1/0, (B) TAA-MW-1.1/10, (C) TAA-MW-1.1/10-magnification, (D) TAA-1.1/0, (E) TAA-1.1/10, and (F) HMDST-1.1/0.

higher amount of TPP exhibit a less uniform appearance. In sample TAA-1.1/0, there are some indications that the spheres could have a hollow structure (see Supporting Information). Such hints are lacking completely in the microwave assisted route. However, a differentiation between closed hollow spheres and fully packed spheres cannot be undertaken from our SEM measurements.

Using HMDST as a precipitation agent, no spherical agglomerates are formed. The powder consists of aggregates of irregular shapes with elongated substructures.

Conclusion

In this paper, we have investigated three different synthesis routes for the preparation of nanocrystalline ZnS powders. XRD measurements reveal a cubic sphalerite structure for all samples with primary crystallite sizes between 1 and 7 nm. This agrees quite well with particle sizes obtained by SAXS. This means that the primary particles are individual crystallites. The low volume fractions indicate a loose packing of the inorganic particles which is caused by the organic capper layers. Comparing the TAA and TAA-MW route, microwave heating increases the primary crystallite size because of the faster decomposition of TAA. Larger crystallites were also obtained by increasing the TAA concentration. Furthermore, for both methods, the presence of TPP leads to smaller crystallites; however, there was no significant dependence of the metal to TPP ratio. By both routes, the main factor lies in the availability of sulfur during the synthesis. The use of HMDST allows the synthesis at room temperature. As the reagent is added dropwise, the concentration of available sulfur is always low, and the smallest primary particle sizes with low polydispersity were obtained. The primary crystallites are aggregated to spherical structures between 650 and 1200 nm.

Acknowledgment. The authors thank Franz Stelzer and Dieter Meissner for helpful discussions. Financial support by the Austrian Research Promotion Agency (FFG) is gratefully acknowledged.

Supporting Information Available: XRD, SAXS curves and data evaluation, representative DLS curves, FTIR spectrum of sample TAA-5/10, and a detailed SEM image of sample TAA-1.1/0. This material is available free of charge via the Internet at http://pubs.acs.org.

IC7017715